Deep-Subwavelength Focusing and Steering of Light in an Aperiodic Metallic Waveguide Array

Lieven Verslegers,* Peter B. Catrysse, Zongfu Yu, and Shanhui Fan†

Ginzton Laboratory and Department of Electrical Engineering, Stanford University, Stanford, California 94305, USA

(Received 6 March 2009; revised manuscript received 16 June 2009; published 15 July 2009)

We consider an aperiodic array of coupled metallic waveguides with varying subwavelength widths. For an incident plane wave, we numerically demonstrate that a focus of as small as one-hundredth of a wavelength can be achieved for a focal distance that is much longer than the wavelength. Moreover, the focusing behavior can be controlled by changing either the incident wavelength or the angle of incidence, thus providing the capability of nanoscale beam steering. We show that the behavior of such subwavelength focusing can be understood using Hamiltonian optics.

DOI: 10.1103/PhysRevLett.103.033902 PACS numbers: 42.82.Et, 73.20.Mf, 73.40.Rw

The study of waveguide array structures has been of fundamental interest in demonstrating optical analogues of semiclassical electron dynamics [1–4], as well as for numerous linear and nonlinear optics applications [5–8]. While most of the earlier studies have focused on dielectric waveguide structures, there has been recent work extending such study to metallic waveguide arrays [9–13]. Compared with dielectric structures, the use of metallic waveguide arrays, with different dispersion characteristics and with each individual waveguide supporting deep-subwavelength modes [14], provides important new opportunities for manipulating light at the nanoscale. For example, periodic metallic waveguide arrays can act as an effective negative index material [9]. When a narrow expanding Gaussian beam impinges on such a planar structure, it negatively refracts and, as a result, shows some focusing inside the structure. Alternatively, a curved input facet can be shown to yield similar focusing behavior [10]. In a different setup, time reversal techniques are used to design a specific wave front to couple light into a periodic metallic waveguide array from the side and achieve deep-subwavelength confinement [11].

In this Letter, we consider an *aperiodic* metallic waveguide array consisting of subwavelength slits in gold, and numerically demonstrate focusing of an incident plane wave into a single slit [Fig. 1]. We also show that the entire focusing behavior can be analytically understood using a Hamiltonian optics approach. In this focusing scheme, for an incident beam at a free space wavelength of λ, most of the incident power can be concentrated into a focal spot with a deep-subwavelength dimension that can be as small as $\lambda/100$ *and* with a focal distance that is several wavelengths long. Therefore, an aperiodic metallic waveguide array enables low-loss deep-subwavelength focusing over a long focal distance, which is of substantial interest in nanophotonics. In contrast to previous works on focusing in metallic waveguide arrays, which all use periodic structures [9–13], our aperiodic approach uses an incident wave that is neither amplitude nor phase modulated to focus most of the incident power into a single slit, with a structure that has a simple planar geometry.

As a concrete example, consider a structure that operates at a wavelength of 1 μm, as shown in Fig. 1(a). At this

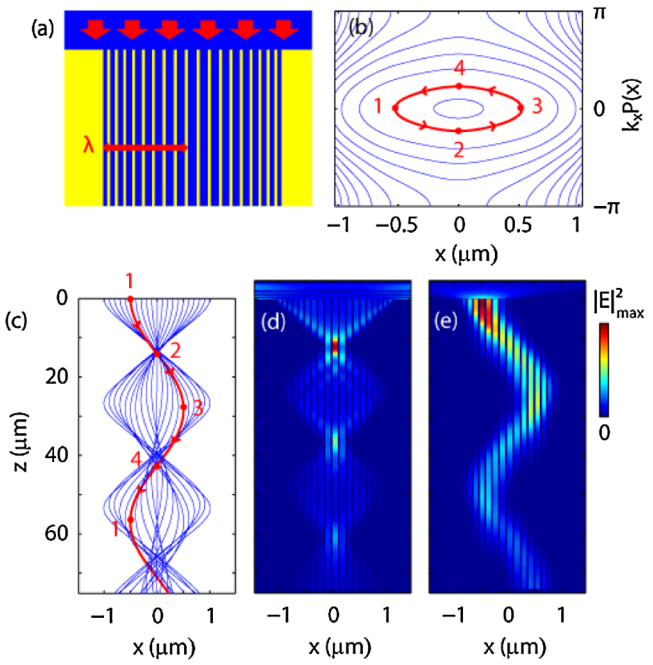

FIG. 1 (color online). Deep-subwavelength focusing with an aperiodic metallic waveguide array. (a) The device geometry: a plane wave (1 μm wavelength) incident upon an aperiodic array of coupled metallic waveguides of varying width (from the side to the center: 46, 54, 62, 70, 78, 84, 90, 94, 98, 100 nm) and constant gold spacing (36 nm). (b) Contour plot of the dispersion relation $k_z(x, k_x)$ throughout the structure; the k_x axis is rescaled (with $P(x)$, the local period) so that for every position x only the first Brillouin zone is shown. (c) Ray tracing inside the structure using Hamiltonian optics. The thick (red) contour and ray are discussed in the main text. FDFD-simulated electric field intensity of the focusing pattern for an incident plane wave (d) and a narrow Gaussian beam (e).

wavelength, the permittivity of gold is $\varepsilon_m = -39.74 + 1.21i$ [15] and the slits support low-loss propagating modes for all considered widths. The slit widths decrease (not linearly) from 100 nm at the center to 46 nm at the sides. Subwavelength gold spacing between the air slits is kept constant at 36 nm. The structure is planar, 2.1 μm wide and semi-infinite in length.

The behavior of this structure can be understood, predicted qualitatively and, to a large degree, even designed for, using Hamiltonian optics [16]. Hamiltonian optics allows one to track rays as they propagate through a structure, given that the dispersion relation is known locally (and does not vary rapidly as a function of position). In order to obtain focusing, we designed a structure for which all rays intersect at the same point, independent of their position of incidence.

Since the dimensions in the aperiodic structure do not vary much from one slit to the adjacent slit, this structure can be thought of approximately as locally periodic. Therefore, at a given frequency ω, the Bloch wave dispersion relation (for transverse magnetic polarization) can be calculated locally using a transfer-matrix formalism [17]:

$$\cos[k_x(a_1 + a_2)] = \cos(k_1 a_1)\cos(k_2 a_2) - \left(\frac{\varepsilon_m^2 k_1^2 + k_2^2}{2\varepsilon_m k_1 k_2}\right) \times \sin(k_1 a_1)\sin(k_2 a_2), \quad (1)$$

with $k_1 = (k_0^2 - k_z^2)^{1/2}$ and $k_2 = (\varepsilon_m k_0^2 - k_z^2)^{1/2}$, where a_1 is the slit width, a_2 is the metal thickness, k_0 is the free space wave vector, and k_z is the propagation wave vector along the z direction, parallel to the slit. For our structure, the exact dispersion relation [Eq. (1)], in fact, matches well with a tight-binding approximation [8,18]:

$$k_z = \frac{\beta_s + \beta_a}{2} + \frac{\beta_s - \beta_a}{2}\cos(k_x P), \quad (2)$$

where β_s and β_a are the symmetric and antisymmetric solutions of k_z in Eq. (1) for $k_x = 0$ and $k_x = \pi/(a_1 + a_2)$, respectively. Equation (2) differs from the dielectric case in that β_s is smaller than β_a (corresponding to a negative coupling constant between neighboring slits.). Note that β_s, β_a and the period P $(= a_1 + a_2)$ are all a function of slit width and therefore, in the aperiodic structure, a function of position x.

The light trajectory in such an aperiodic structure can be calculated using the Hamiltonian optics formalism, in which a Hamiltonian can be directly derived from the dispersion relation [Eq. (2)] as:

$$H(x, k_x) = k_z - \frac{\beta_s(x) + \beta_a(x)}{2} - \frac{\beta_s(x) - \beta_a(x)}{2} \times \cos[k_x P(x)]. \quad (3)$$

Here β_s, β_a and P were calculated for each slit width in the lossless periodic structure and then fitted as a function of position x with a polynomial. Figure 1(b) represents solutions to $H(x, k_x) = 0$ for different k_z values. As a result of continuous translational symmetry along z, k_z is a conserved quantity; thus, every contour in Fig. 1(b), which is at a constant k_z, corresponds to a light trajectory in real space.

From the Hamiltonian of Eq. (3), the trajectory of a ray in the structure can be solved using:

$$\frac{dx}{dz} = \frac{\partial H(x, k_x)}{\partial k_x}, \qquad \frac{dk_x}{dz} = -\frac{\partial H(x, k_x)}{\partial x}. \quad (4)$$

Figure 1(c) shows the trajectories of several rays that have no initial lateral momentum ($k_x = 0$), corresponding to a perpendicularly incident plane wave. We link the flow in Hamiltonian phase space to the propagation in real space for one position of incidence [the thick (red) contour in Fig. 1(b) and the thick (red) ray in Fig. 1(c)]. We note that the ellipse gets traversed in counterclockwise direction. This means that when the k_x wave vector points in one direction, light moves in the opposite x direction. Hence this structure exhibits negative refraction [9]. This will be shown in more detail below for rays that are incident under an angle.

We can analytically describe the ray trajectory if we approximate the Hamiltonian to second order in k_x and x, which requires parabolic fits: $\beta_s(x) = \beta_{s,0} + \beta_{s,2}x^2$; $\beta_a(x) = \beta_{a,0} + \beta_{a,2}x^2$ and $P(x) = P_0 + P_2 x^2$. In this approximation, the Hamiltonian can be written as

$$H(x, k_x) = k_z - \beta_{s,0} - \beta_{s,2}x^2 + \frac{1}{4}(\beta_{s,0} - \beta_{a,0})P_0^2 k_x^2. \quad (5)$$

The phase space contour is then exactly an ellipse. As a result, the ray goes through a sinusoidal trajectory as it propagates along the z direction

$$x(z) = C_1 \sin\{[(\beta_{a,0} - \beta_{s,0})\beta_{s,2}]^{1/2} P_0 z\} + C_2 \cos\{[(\beta_{a,0} - \beta_{s,0})\beta_{s,2}]^{1/2} P_0 z\}, \quad (6)$$

with C_1 and C_2 depending on the position and angle of the incident ray. Importantly, the period of $x(z)$

$$z_{\text{period}} = \frac{2\pi}{[(\beta_{a,0} - \beta_{s,0})\beta_{s,2}]^{1/2} P_0} \quad (7)$$

is independent of the position of incidence, i.e., independent of $x(z = 0)$. As a result, for a normally incident plane wave all rays intersect at a focal length that is a quarter of z_{period}.

We confirm the analytical results by comparing them to finite-difference frequency-domain (FDFD) simulations [19], which solves the underlying Maxwell's equations with no uncontrolled approximation. In FDFD, we calculate the electromagnetic fields by solving a large sparse linear system derived from Maxwell's equations. This method allows us to model materials using the measured, tabulated permittivity for every wavelength, thus directly taking into account both material dispersion as well as loss. In all our simulations, we set the grid size to 1–2 nm in the transverse x direction and 40–80 nm in the longitudinal z

direction. This enables us to model the very fine features of the field at the metal-air interfaces inside the slits while maintaining a reasonable simulation domain size.

Figure 1(d) shows the electric field intensity pattern of the structure for an incident plane wave. The behavior is in good agreement with the predictions from Hamiltonian optics. The transverse focal spot is an order of magnitude smaller than the wavelength, since light is confined mostly in the 100 nm wide center slit. This focusing occurs over a length scale that corresponds to multiple wavelengths. Equation (7) predicts a focal length of 11.1 μm, close to the simulated result. Past the focus, the pattern expands again to the full width of the structure. This pattern reproduces itself, albeit weakened by metallic losses. Essentially, this metallic waveguide array acts as a harmonic oscillator for light. This behavior is reminiscent of a graded-index lens, albeit one with a more complex dispersion relation.

In Fig. 1(e), we show the response when the aperiodic structure is excited locally with a Gaussian profile that has a full width at half maximum (FWHM) of half the wavelength at the entrance surface. The resulting electric field intensity profile corresponds quite well to the highlighted ray from Hamiltonian optics, thus providing a direct visual validation of the Hamiltonian optics in this nanoscale system. (As a side note, this is not a Bloch oscillation, since the edge of the Brillouin zone is never reached for this ray.)

The focusing effect introduced can be achieved over a wide range of frequencies. To operate at a longer wavelength, one needs to use narrower slits and gold spacing to enhance interaction between neighboring slits, since for a fixed gold spacing and slit width the coupling between waveguides decreases as the wavelength increases. We demonstrate focusing at longer wavelengths of 2–4 μm in Fig. 2, using a structure with a total of 41 slits that vary linearly in width from 10 to 30 nm from the sides to the center, separated by 20 nm gold.

The focal length can be controlled by tuning the wavelength. In Figs. 2(a)–2(c) the focal length increases from 12.1 μm (at 2 μm, $\varepsilon_m = -178.15 + 7.13i$) over 19.0 μm (at 3 μm, $\varepsilon_m = -408.35 + 22.58i$) to 25.9 μm (at 4 μm, $\varepsilon_m = -729.75 + 50.83i$). The focusing of 3 μm wavelength light to a 30 nm slit corresponds to a focal spot of one-hundredth of a wavelength, as calculated using a FWHM criterion. At the focus, the z-directed flux is 57.3% of the flux that has entered the structure over the width of the structure at the entrance plane. The transmission at the interface of the entrance plane is 89.2%; thus most of the loss is due to the metal absorption. The results again correspond well to Hamiltonian optics [Figs. 2(d)–2(f)]. Equation (7) predicts focal lengths that are slightly longer, but close to the ones from simulations: 13.8 μm, 21.0 μm and 28.1 μm. For this same structure, we still observe focusing behavior at 10 μm wavelength (not shown).

We also show the ability of this structure (from Fig. 2) to perform lateral nanoscale steering of the focal spot. Specifically, the focal spot can be steered laterally from slit to slit, by tilting the incident plane wave. Figures 3(a)–3(c) show an incident beam at 1.55 μm wavelength ($\varepsilon_m = -104.31 + 3.68i$) steered from the first to the second and third slit, as counted from the center, by varying the incident angles of, respectively, 0, 23 and 44 degrees. The focus spot moves away from the direction in which the beam is tilted, as a result of the negative refraction behavior of this system. These observations are in good agreement with what Hamiltonian optics predicts [Figs. 3(d)–3(f)].

From the theoretical point of view, our results indicate the importance of Hamiltonian optics for understanding the behavior of aperiodic nanoscale plasmonic structures. We note that the success of Hamiltonian optics relies on the large difference in terms of length scale between the optical beam size and the underlying structural periodicity. In

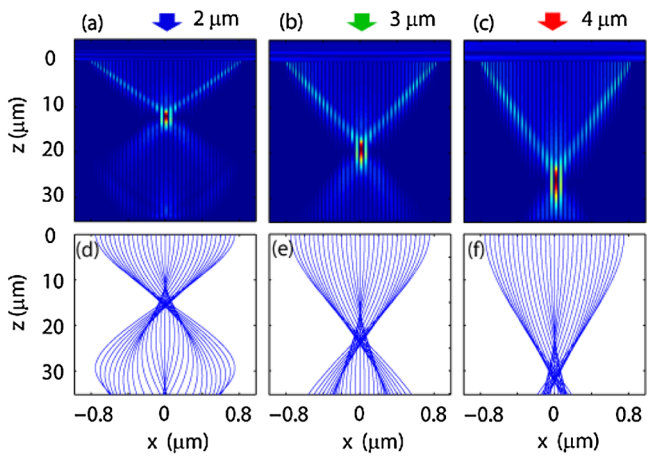

FIG. 2 (color online). Focusing in an aperiodic metallic waveguide array at longer wavelengths. FDFD simulations (a)–(c), Hamiltonian optics (d)–(f).

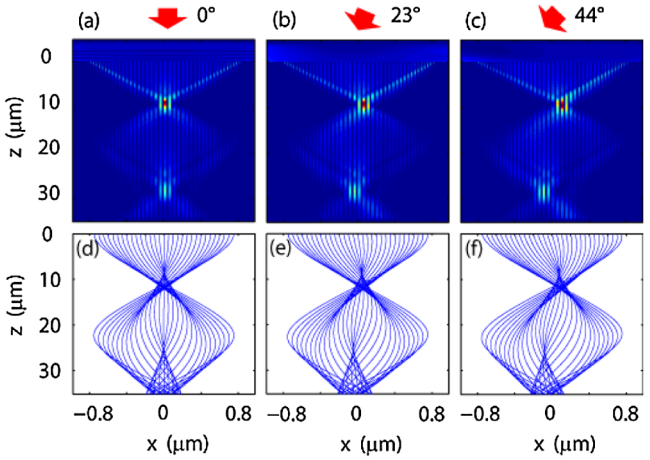

FIG. 3 (color online). Lateral nanosteering with an aperiodic metallic waveguide array. FDFD simulations (a)–(c), Hamiltonian optics (d)–(f).

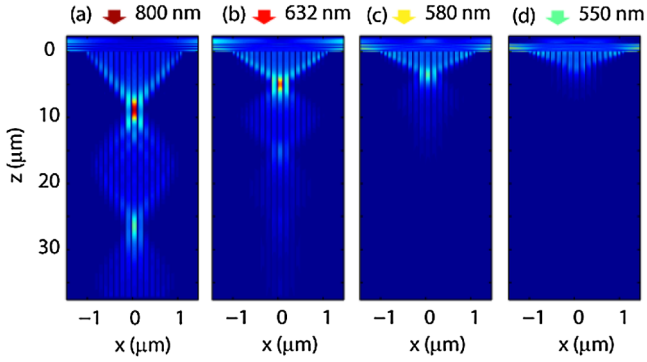

FIG. 4 (color online). Focusing with the aperiodic metallic waveguide array from Fig. 1 at shorter and visible wavelengths.

traditional dielectric structures such as photonic crystals, since the underlying periodicity is comparable to the wavelength, Hamiltonian optics is applicable only for beams with transverse dimensions much larger than the wavelength [16,20,21]. In the structures considered here, however, the underlying structure has a periodicity that is much smaller than the wavelength. Thus, in plasmonic structures, Hamiltonian optics can be used to predict many of the important characteristics that are at a single wavelength, or even subwavelength scale.

In concluding, we briefly discuss losses in these structures. In general, losses will increase when slits are spaced further apart. However, one cannot space the slits too closely, since one needs to rely upon the metal region between the slits to provide the capability for subwavelength light confinement. Losses can be contained by keeping the focal distance short. In periodic structures, there exists a maximum angle of propagation $\alpha \approx 2CP$, with C the coupling constant between two adjacent waveguides and P the period [18]. As an example, the calculated maximum angles for the structure in Fig. 3 (1.55 μm light) range from 5.7 to 6.8 degrees. For wide structures, the focal length will be long and, consequently, losses will be significant. Thus, the ideal operating mode of our structure is to focus a wavelength scale beam into a deep-subwavelength spot.

All wavelengths considered thus far in this Letter lie in the infrared. The focusing effect in the visible is illustrated in Fig. 4. The structure considered is the same as the one in Fig. 1; the wavelengths are 800 nm ($\varepsilon_m = -22.72 + 0.76i$), 632 nm ($\varepsilon_m = -10.73 + 0.79i$), 580 nm ($\varepsilon_m = -7.38 + 1.09i$) and 550 nm ($\varepsilon_m = -5.31 + 1.37i$) [Figs. 4(a)–4(d)]. Focusing is still observed for wavelengths down to 580 nm. The focusing effect, as measured by the field intensity enhancement (as compared to an incident plane wave), however, becomes less pronounced at shorter wavelengths due to losses near the gold resonance. Indeed, the field intensity enhancement in the center slit at focus is 8.3 at 800 nm, 4.9 at 632 nm, and 2.4 at 580 nm. For even shorter wavelengths, no real focusing (i.e., enhancement) is observed for this structure, as light is attenuated faster than it is concentrated.

These novel planar structures, with their ability to focus and steer over a wide range of wavelengths, can find applications in wavelength division multiplexing, spectroscopy, and lithography. For lithography purposes, for example, one could envision truncating the structure at the focal point and using the near field resulting from such focal point. Since they are essentially one dimensional, these structures can be deposited in a layer-by-layer fashion, whereby the air slits are replaced by dielectric layers. The presented design principles based on Hamiltonian optics should be generalizable for more complex plasmonic structures.

This research was supported by Sharp Labs of America, and by an AFOSR MURI program on plasmonics. (FA9550-04-1-0437).

*Lievenv@stanford.edu
†Shanhui@stanford.edu

[1] R. Morandotti *et al.*, Phys. Rev. Lett. **83**, 4756 (1999).
[2] G. Lenz, I. Talanina, and C. M. de Sterke, Phys. Rev. Lett. **83**, 963 (1999).
[3] U. Peschel, T. Pertsch, and F. Lederer, Opt. Lett. **23**, 1701 (1998).
[4] R. Khomeriki and S. Ruffo, Phys. Rev. Lett. **94**, 113904 (2005).
[5] D. N. Christodoulides, F. Lederer, and Y. Silberberg, Nature (London) **424**, 817 (2003).
[6] A. Yariv, IEEE J. Quantum Electron. **9**, 919 (1973).
[7] H. A. Haus, L. Molter-Orr, and F. J. Leonberger, Appl. Phys. Lett. **45**, 19 (1984).
[8] D. N. Christodoulides and R. I. Joseph, Opt. Lett. **13**, 794 (1988).
[9] X. Fan *et al.*, Phys. Rev. Lett. **97**, 073901 (2006).
[10] X. Fan and G. P. Wang, Opt. Lett. **31**, 1322 (2006).
[11] G. Bartal, G. Lerosey, and X. Zhang, Phys. Rev. B **79**, 201103(R) (2009).
[12] M. Conforti, M. Guasoni, and C. De Angelis, Opt. Lett. **33**, 2662 (2008).
[13] Z. Kang and G. P. Wang, J. Opt. Soc. Am. B **25**, 1984 (2008).
[14] E. N. Economou, Phys. Rev. **182**, 539 (1969).
[15] *CRC Handbook of Chemistry and Physics*, edited by D. R. Lide (CRC Press, Boca Raton, FL, 2007), 88th ed..
[16] P. St. J. Russell and T. A. Birks, J. Lightwave Technol. **17**, 1982 (1999).
[17] A. Yariv and P. Yeh, *Photonics: Optical Electronics in Modern Communications* (Oxford University Press, New York, NY, 2006), 6th ed..
[18] H. S. Eisenberg *et al.*, Phys. Rev. Lett. **85**, 1863 (2000).
[19] G. Veronis and S. Fan, in *Surface Plasmon Nanophotonics*, edited by M. L. Brongersma and P. G. Kik (Springer, New York, 2007), pp. 169–182.
[20] Y. Jiao, S. Fan, and D. A. B. Miller, Phys. Rev. E **70**, 036612 (2004).
[21] P. Stellman, K. Tian, and G. Barbastathis, CLEO/QELS, Baltimore Report No. JThD121, 2007.